

Acetic Acid Aldose Reductase Inhibitors Bearing a Five-Membered Heterocyclic Core with Potent Topical Activity in a Visual Impairment Rat Model

Concettina La Motta,^{*,†} Stefania Sartini,[†] Silvia Salerno,[†] Francesca Simorini,[†] Sabrina Taliani,[†] Anna Maria Marini,[†] Federico Da Settimo,[†] Luciana Marinelli,[‡] Vittorio Limongelli,[‡] and Ettore Novellino[‡]

Dipartimento di Scienze Farmaceutiche, Università di Pisa, Via Bonanno 6, 56126 Pisa, Italy, Dipartimento di Chimica Farmaceutica e Tossicologica, Università di Napoli "Federico II", Via D. Montesano 49, 80131 Napoli, Italy

Received December 21, 2007

A number of 1,2,4-oxadiazol-5-yl-acetic acids and oxazol-4-yl-acetic acids were synthesized and tested for their ability to inhibit aldose reductase (ALR2). The oxadiazole derivatives, **7c**, **7f**, **7i**, and **8h**, **8i**, proved to be the most active compounds, exhibiting inhibitory levels in the submicromolar range. In this series, the phenyl group turned out to be the preferred substitution pattern, as its lengthening to a benzyl moiety determined a general reduction of the inhibitory potency. The lead compound, 2-[3-(4-methoxyphenyl)-1,2,4-oxadiazol-5-yl]acetic acid, **7c**, showed an excellent in vivo activity, proving to prevent cataract development in severely galactosemic rats when administered as an eye-drop solution in the precorneal region of the animals. Computational studies on the ALR2 inhibitors were performed to rationalize the structure–activity relationships observed and to provide the basis for further structure-guided design of novel ALR2 inhibitors.

Introduction

Aldose reductase (alditol:NADP⁺ 1-oxidoreductase, EC 1.1.1.2, ALR2) is a small, cytosolic, monomeric enzyme of 36 kDa. It belongs to the aldo-keto reductase (AKR) superfamily and catalyzes the NADPH-dependent reduction of a wide variety of medium- to long-chain aldehydes to their corresponding alcohols, exhibiting a broad substrate specificity. ALR2 plays a pivotal role in the development of long-term diabetic complications, as a wealth of experimental data clearly demonstrate.^{1–4} It is the key enzyme of the polyol pathway and catalyzes the reduction of glucose to sorbitol, which is then oxidized to fructose by sorbitol dehydrogenase (L-iditol:NAD⁺, 5-oxidoreductase, EC 1.1.1.14, SD). As ALR2 has a low substrate affinity for glucose, the conversion of glucose to sorbitol through the polyol pathway is generally nonsignificant in normoglycemic conditions, accounting for no more than 3% of total glucose utilization. In fact, ALR2 must compete directly with the hexokinase of the glycolytic pathway, and as the substrate affinity of hexokinase is greater than that of ALR2, glucose is preferentially phosphorylated into glucose-6-phosphate. Conversely, under hyperglycemic conditions, hexokinase is rapidly saturated and the polyol pathway becomes activated. Sorbitol is formed more rapidly than it is converted to fructose,

and its polarity hinders an easy penetration through membranes and subsequent removal from tissues by diffusion. The resulting elevated intracellular concentration of sorbitol increases cellular osmolarity, which in turn initiates a cascade of events that lead to the development of disabling complications, peculiar of diabetic disease and affecting the nervous, cardiovascular, renal, and visual systems. In addition to the osmotic imbalance, an increase in the activity of ALR2 during hyperglycemia causes a substantial imbalance in the free cytosolic coenzyme ratios NADPH/NADP⁺ and NAD⁺/NADH. This alteration in the redox state of pyridine nucleotides induces a state of pseudo-hypoxia, which contributes to the onset of hyperglycemic oxidative stress through the accumulation of reactive oxygen species (ROS). ROS, in turn, trigger activation of downstream mechanisms, namely, protein kinase C (PKC) isoforms, mitogen-activated protein kinases (MAPKs) and poly(ADP-ribose)-polymerase (PARP), as well as the inflammatory cascade, which sustain the pathogenesis of diabetic complications.^{5–10} Inhibition of ALR2 is therefore a useful therapeutic strategy to prevent the onset or, at least, delay the progression and the severity of diabetic complications.

Many compounds have been shown to inhibit ALR2 with varying degrees of efficacy and selectivity (Chart 1).^{11–13} Although chemically different, they all share common structural features, represented by a wide lipophilic, aromatic area and a ionizable group. These moieties turn out to be essential for an effective interaction with the binding site of the enzyme, which appears as divided into two distinct portions: a "catalytic subpocket" and a "specificity pocket". The ionizable group of the inhibitor anchors it to the "catalytic subpocket" through hydrogen bond interactions with two polar amino acid residues, namely Tyr48 and His110. As a result, the lipophilic scaffold of the molecule turns out to be oriented within the hydrophobic, highly plastic "specificity pocket", which exhibits a high degree of induced-fit adaptation and can potentially host a wide range of structures.¹⁴

Despite the impressive number of compounds described as effective ALR2 inhibitors (ARIs), a true and widespread ARI

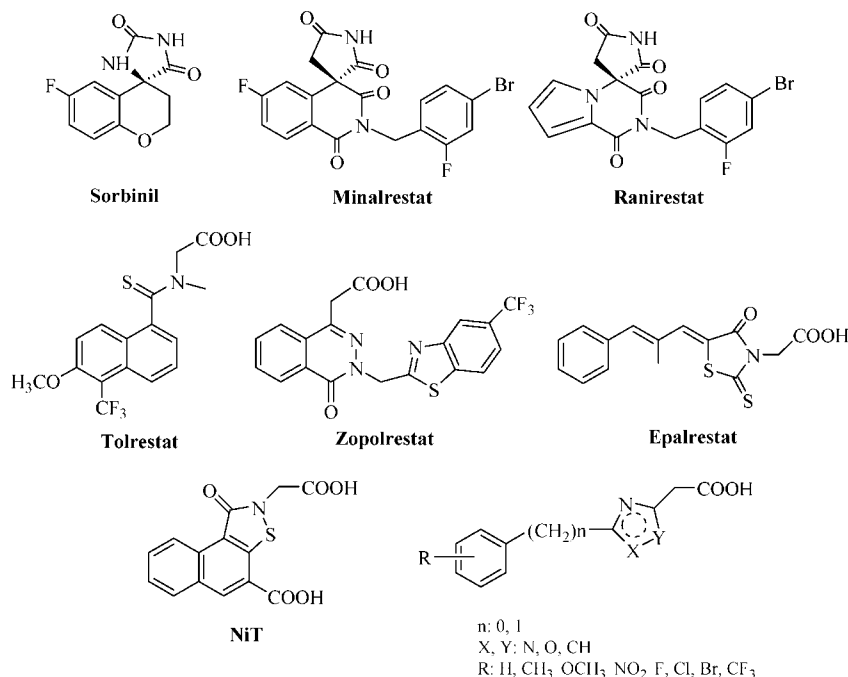
* To whom all correspondence should be addressed. Phone: (+)390502219593. Fax: (+)390502219605. E-mail: lamotta@farm.unipi.it.

[†] Dipartimento di Scienze Farmaceutiche, Università di Pisa.

[‡] Dipartimento di Chimica Farmaceutica e Tossicologica, Università "Federico II" di Napoli.

^a Abbreviations: NADP⁺, β -nicotinamide adenine dinucleotide phosphate; ALR2, aldose reductase; AKR, aldo-keto reductase; NAD⁺, β -nicotinamide adenine dinucleotide; SD, sorbitol dehydrogenase; NADPH, β -nicotinamide adenine dinucleotide phosphate reduced form; NADH, β -nicotinamide adenine dinucleotide reduced form; ROS, reactive oxygen species; PKC, protein kinase C; MAPK, mitogen-activated protein kinase; PARP, poly(ADP-ribose)polymerase; ARI, aldose reductase inhibitor; HNE, hydroxynonenal; AGEs, advanced glycation end products; ALR1, aldehyde reductase; NIT, 3,3-dioxide-1,2-dihydronaphtho[1,2-*d*]isothiazol-1-one; SAR, structure–activity relationship; ClogP, calculated *n*-octanol/water partition coefficient; ClogD, calculated distribution coefficient; TPSA, topological polar surface area.

Chart 1. Aldose Reductase Inhibitors

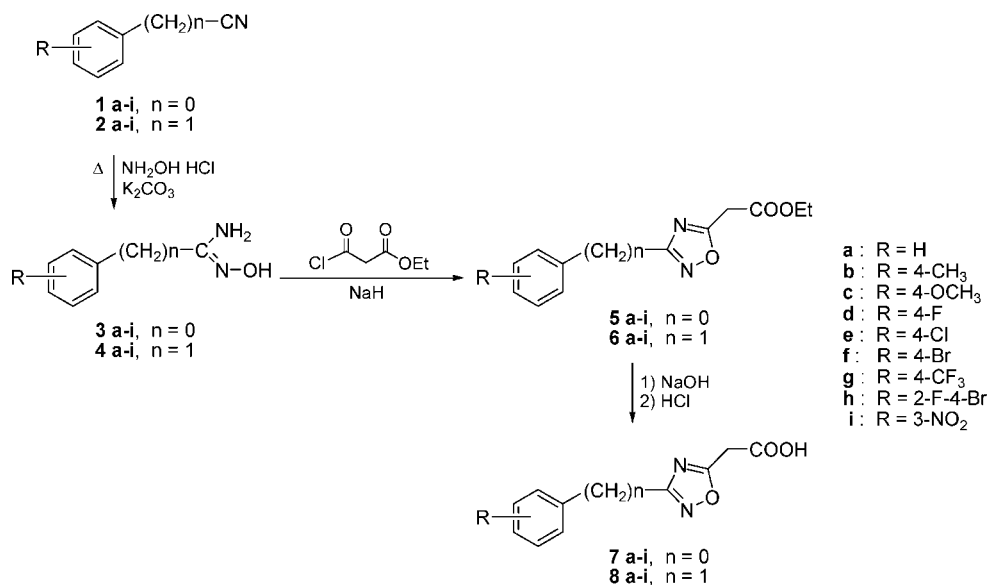


therapy is not yet an established fact, seeing that to date, only epalrestat is successfully marketed for treatment of diabetic neuropathy in Japan. Products that appear to be promising during *in vitro* studies or in trials with animal models often fail to proceed any further, showing uncertain results in clinical trials with humans. This failure is generally due to either a limited efficacy or the emergence of adverse side effects. The former is often caused by an inappropriate dosing schedule of the inhibitor or by an unfitting pharmacokinetic, tethered with its absorption, distribution, metabolism, and excretion properties. The latter are mainly a consequence of the important physiological role performed by the enzyme. Actually, besides the polyol pathway, ALR2 shows other activities, mostly linked to oxidative defense mechanisms. This enzyme is highly efficient in reducing toxic aldehydes such as hydroxynonenal (HNE), methyl glyoxale, and 3-deoxyglucosone, which arise in large quantities from pathological conditions connected with oxidative stress and are responsible for the formation of protein cross-links and advanced glycation end products (AGEs). ALR2 also catalyzes the reduction of glutathione conjugates of unsaturated aldehydes, showing in most cases an efficiency higher than that of the parent compound, free aldehyde.^{15–17} ALR2 therefore ensures a complete and efficient removal of the major electrophilic end products of lipid peroxidation, playing a significant aldehyde removal function, which becomes highly relevant under particular conditions of oxidative stress when other antioxidant mechanisms are overwhelmed. ALR2 shares its detoxification role with aldehyde reductase (EC 1.1.1.2, ALR1), a closely related enzyme. Both ALR2 and ALR1 belong to the AKR superfamily possessing the highest structural homology, with 65% identity in their amino acid sequences.¹⁸ The least conserved residues are located at the C-terminal end of the proteins in a region lining the hydrophobic specificity pocket. This portion of the active site is responsible for the substrate and inhibitor specificity of the two enzymes and can therefore be usefully exploited for the design of selective compounds, which must be able to inhibit ALR2 without affecting the detoxification activity of ALR1.^{19–21}

Thus, clinically effective and safe therapies to prevent long-term diabetic complications can be achieved through the development of novel ARIs, which necessarily must combine high levels of efficacy and selectivity with suitable pharmacokinetic properties.

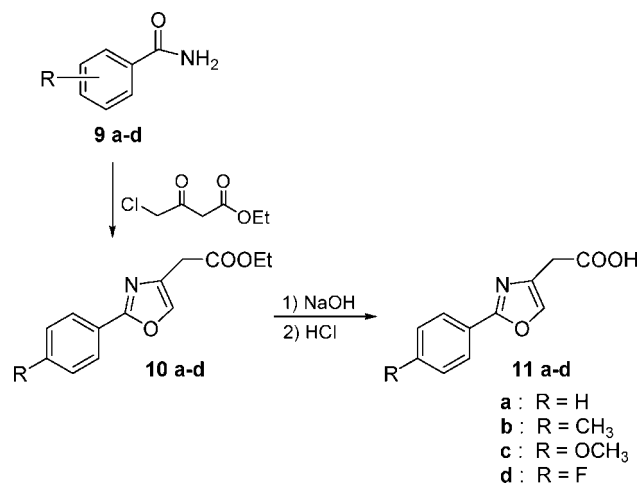
Our research group has been working in the ARI field for many years^{22–26} with the aim of disclosing novel drugs that are candidates for the topical treatment of diabetic visual impairments, which are the leading cause of blindness in people aged from 20 to 75. We have identified structurally different inhibitors, one of the latest being acetic acid derivatives of 3,3-dioxide-1,2-dihydronaphtho[1,2-*d*]isothiazol-1-one (NiT), which proved to be relatively potent inhibitors, showing IC_{50} values in the micromolar/submicromolar range (Chart 1).²⁵ These compounds made it possible to disclose a novel and unexpected binding mode to the active site of the enzyme, confirming once more the high plasticity of ALR2. X-ray analysis of the enzyme crystal structure complexed with the most active NiT derivative revealed the opening of a novel subpocket, never highlighted before, which hosts the naphthyl portion of the scaffold, extending the catalytic subpocket of the active site.^{27,28}

The most active NiT inhibitor was also investigated *in vivo* for its ability to prevent cataract development, the major visual complication of diabetic disease. Despite its good *in vitro* inhibitory potency, this compound did not show any significant efficacy. When administered as a 3% eye-drop solution in the precorneal region of severely galactosemic rats, it failed to prevent lens degeneration. On the contrary, converted to a suitable isopropyl ester prodrug, it exhibited an excellent activity, proving to protect 55% of the animals treated from cataract development when administered with the same dose regimen. These results suggest that the NiT compound, as a carboxylic acid, possesses a poor ocular absorption that prevents it from reaching the lens, the intraocular site of action. It is well-known that many factors compete with the ocular absorption of a topically applied drug. They include rapid drainage from the application site, induced lachrymation, tear turnover, and corneal permeability, this latter being the prominent one. The cornea

Scheme 1. Synthesis of 3-Aryl-1,2,4-oxadiazol-5-yl-acetic Acids **7a–i** and **8a–i**

represents the major pathway for drug penetration, and in terms of permeability it can be considered as consisting of three primary layers: epithelium, stroma, and endothelium. Both the epithelium and the endothelium are lipophilic and constitute the main barriers for hydrophilic compounds. The stroma is an aqueous layer, thus limiting permeability of lipophilic compounds. Therefore, the ability of a drug to penetrate through the cornea is strictly dependent on its hydrophilic–lipophilic properties, which must be adequately balanced. Carboxylic-type compounds are almost completely in their ionized form at physiological pH values. Therefore, they generally exhibit a low *in vivo* activity due to an unfavorable tissue penetration. However, a number of literature examples, also in the ARI field,²⁹ demonstrate that the pharmacokinetic properties of these compounds can be optimized in order to improve their permeability profile. Moving from these observations, we planned to realize appropriate structural modifications of the NiT scaffold in order to design a simpler molecular skeleton possessing a favorable pharmacokinetic profile, suitable for ocular tissue penetration. Thus, removing the central phenyl ring from the naphtho[1,2-*d*]isothiazole nucleus, we obtained five-membered ALR2 inhibitors, possessing an acetic acid function and a hydrophobic group. On the basis of synthetic feasibility and, above all, on the basis of previously reported works by G. Klebe and co-workers on similar structures,^{30,31} we targeted two different five-membered rings, namely 1,2,4-oxadiazole and oxazole, as suitable candidates for the development of novel inhibitors.

In this work, we present the synthesis and an extensive biological evaluation of a number of oxadiazole and oxazole acetic acid derivatives. To clearly define the structure–activity relationships (SARs) of the two classes of inhibitors, suitable substituted phenyl or benzyl groups were introduced into position 3 of the oxadiazole ring and position 2 of the oxazole ring. Moreover, compound **7c**, which proved to be the most active of all, was also investigated *in vivo* in view of its ability to prevent cataract development in severely galactosemic rats. Molecular docking simulations of the most potent inhibitors into the human ALR2 binding site were also carried out in order to propose the mode of binding of these compounds, which turned

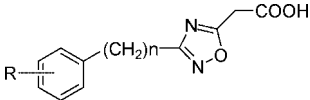
Scheme 2. Synthesis of 2-(2-Phenylloxazol-4-yl)acetic Acids **11a–d**

out to be fully consistent with the SARs observed and helped to rationalize them.

Chemistry

The synthesis of the target 1,2,4-oxadiazole inhibitors **7a–i** and **8a–i** was performed as outlined in Scheme 1. The appropriately substituted nitriles **1a–i** and **2a–i** were treated with hydroxylamine hydrochloride, in the presence of potassium carbonate, to give the *N*-hydroxybenzimidamide and *N*-hydroxy-2-phenylacetimidamide intermediates **3a–i** and **4a–i**, respectively. Condensation of **3a–i** and **4a–i** with ethyl 3-chloro-3-oxopropanoate, in the presence of sodium hydride, provided the ethyl esters **5a–i** and **6a–i**, which were then hydrolyzed with boiling sodium hydroxide to obtain, after acidification, the desired acids **7a–i** and **8a–i**.

The oxazole inhibitors **11a–d** were prepared as reported in Scheme 2, in accordance with a literature procedure.³² Reaction of the commercially available benzamides **9a–d** with ethyl 4-chloro-3-oxobutanoate led to the ethyl esters **10a–d**. Hy-

Table 1. ALR2 Inhibition Data of [1,2,4]oxadiazol-5-yl-acetic Acids **7a–i** and **8a–i**


N	n	R	ALR2 IC ₅₀ (μM) ^a	ALR1 IC ₅₀ (μM) ^a
7a	0	H	3.33 (2.83–3.83)	> 10 μM
7b	0	4-CH ₃	2.50 (2.05–2.95)	> 10 μM
7c	0	4-OCH ₃	0.27 (0.23–0.31)	> 10 μM
7d	0	4-F	8.43 (6.75–10.11)	> 10 μM
7e	0	4-Cl	3.95 (3.16–4.74)	> 10 μM
7f	0	4-Br	0.69 (0.61–0.77)	> 10 μM
7g	0	4-CF ₃	1.08 (0.88–1.28)	> 10 μM
7h	0	2-F-4-Br	2.00 (1.65–2.36)	> 10 μM
7i	0	3-NO ₂	0.71 (0.63–0.79)	> 10 μM
8a	1	H	28.4 (22.44–33.36)	> 10 μM
8b	1	4-CH ₃	5.29 (4.24–6.34)	> 10 μM
8c	1	4-OCH ₃	8.18 (6.71–9.65)	> 10 μM
8d	1	4-F	21.7 (17.8–25.6)	> 10 μM
8e	1	4-Cl	5.11 (4.35–5.87)	> 10 μM
8f	1	4-Br	1.66 (1.43–1.89)	> 10 μM
8g	1	4-CF ₃	6.30 (5.23–7.37)	> 10 μM
8h	1	2-F-4-Br	0.36 (0.33–0.39)	> 10 μM
8i	1	3-NO ₂	0.30 (0.22–0.37)	> 10 μM
Tolrestat			0.05 (0.03–0.06)	> 10 μM

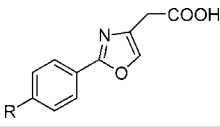
^a IC₅₀ (95% CL) values represent the concentration required to produce 50% enzyme inhibition.

drolisis of **10a–d** under alkaline medium afforded, after acidification, the target compounds **11a–d**.

Results and Discussion

Biological Evaluation. We started this research project by synthesizing a number of 3-phenyl-1,2,4-oxadiazol-5-yl-acetic acid derivatives, **7a–i**, and testing them for their efficacy against ALR2 and selectivity for ALR1. Within this series, different substituents were introduced in various positions around the phenyl ring in order to verify the influence of electron-withdrawal, electron-release, steric bulk, and orientation on the inhibitory potency of these molecules. As shown in Table 1, which lists the activity against ALR2 expressed as IC₅₀ values, all the compounds synthesized proved to inhibit this enzyme, exhibiting potency levels in the micromolar/submicromolar range. The insertion of electron-donating substituents in the para position of the 3-phenyl group determined a general increase in the inhibitory potency with respect to the unsubstituted parent compound **7a** (IC₅₀ 3.33 μM). Actually, derivative **7b**, bearing a methyl group, showed an IC₅₀ value of 2.50 μM and derivative **7c**, carrying a methoxy substituent, proved to be extremely potent, with an IC₅₀ value of 0.27 μM and a gain in inhibitory potency of 12-fold when compared to the lead **7a**.

The presence of electron-withdrawing, halogen atoms in the same position as the pendant phenyl ring gave rise to opposite but not contrasting results. In fact, moving from the less bulky, more electron-attracting halogen to the bulkier, less electron-attracting one, we observed a progressive enhancement in the IC₅₀ values of the corresponding compounds, which moved from 8.43 μM for derivative **7d** to 3.95 μM for **7e** and to 0.69 μM for **7f**, bearing a fluoro, chloro, and bromo atom, respectively. Clearly, the size and the electronic feature of the halogen atom affected the binding affinity of these molecules considerably, allowing for each of them a different interaction with the enzyme. The insertion of the bulkier trifluoromethyl group broke off this positive trend, as derivative **7g** showed an IC₅₀ value of 1.08 μM. Compound **7h** (IC₅₀ 2.00 μM), featuring the *ortho*-fluoro *para*-bromo substitution pattern typical of potent ARI

Table 2. ALR2 Inhibition Data of Oxazol-4-yl-acetic Acids **11a–d**


N	R	ALR2 IC ₅₀ (μM) ^a
11a	H	n.a. ^b
11b	CH ₃	n.a. ^b
11c	OCH ₃	54.8 (46.58–63.02)
11d	F	n.a. ^b
Tolrestat		0.05 (0.03–0.06)

^a IC₅₀ (95% CL) values represent the concentration required to produce 50% enzyme inhibition. ^b n.a.: not active. Inhibition occurred at a concentration higher than 100 μM.

such as Ponalrestat,³³ ranirestat,³⁴ and minalrestat,³⁵ displayed a good activity as well, although it was less potent than the bromo-substituted **7f**. Finally, the insertion of a nitro group in the meta position of the phenyl ring, as in **7i** (IC₅₀ 0.71 μM), determined a 5-fold enhancement in potency with respect to the parent compound **7a**, confirming the fruitful contribution of this type of substituent to the interaction with the amino acid residues surrounding the ALR2 active site, as previously observed by G. Klebe and co-workers for similar inhibitors.³¹

To explore the effects of increasing the distance between the pendant 3-phenyl ring and the five-membered heterocyclic core, a methylene spacer was inserted between them to give derivatives **8a–i** (Table 1). This distance appeared to be a crucial element in determining the best spatial relationship between the pharmacophoric groups of these compounds. The lengthened derivatives were generally less active than the shorter ones, with the only exception of **8h,i**, which exhibited a better inhibitory activity than the parent **7h,i**. However, the novel compounds displayed parallel SARs to those of series **7**: the insertion of electron-donating substituents in the para position of the benzyl framework, as in derivatives **8b** (R = CH₃, IC₅₀ 5.29 μM) and **8c** (R = OCH₃, IC₅₀ 8.18 μM), determined an appreciable increase in the inhibitory efficacy with respect to the unsubstituted compound, **8a** (IC₅₀ 28.4 μM), and the presence of a halogen atom provided a rank order of inhibitory potency fluoro (**8d**, IC₅₀ 21.7) < chloro (**8e**, IC₅₀ 5.11) < bromo (**8f**, IC₅₀ 1.66) > trifluoromethyl (**8g**, IC₅₀ 6.30). In contrast to the 3-phenyl series **7**, the presence of two halogen atoms in the *ortho* and *para* positions of the benzyl group determined a remarkable enhancement in the inhibitory activity. Compound **8h** proved to be highly potent, with an IC₅₀ value of 0.36 μM and a 80-fold increase in efficacy with respect to the lead **8a**. In addition, the introduction of a nitro substituent in the meta position of the 3-benzyl group gave **8i** (IC₅₀ 0.30 μM), which proved to be the most active of the whole series. These results confirm once more the positive effect of this substitution pattern in a specific and forceful interaction with the enzyme active site.

Finally, to investigate the role played by the oxadiazole heterocyclic fragment of the inhibitor template in the interaction with the enzyme, a number of oxazol-4-yl-acetic acids derivatives, **11a–d**, were likewise synthesized and tested. As summarized in Table 2, none of them proved to inhibit ALR2 significantly, with the only exception of the *para*-methoxy substituted **11c** (IC₅₀ 54.8 μM), which, although effective, displayed a 200-fold decrease in inhibitory potency when compared to the corresponding oxadiazole **7c**.

All the compounds synthesized, **7a–i**, **8a–i**, and **11c**, were assayed for their ability to inhibit ALR1, but none of them showed any appreciable activity (IC₅₀ > 10 μM, Table 1), proving to be completely selective inhibitors of ALR2.

Table 3. Physicochemical Property Predictions of Compounds **7c,f,g,i, 8f,h,i**, and Tolrestat

N	pK _a ^a (M)	ClogP ^b	ClogD ^c	TPSA ^d (Å)
7c	4.149	0.40	-1.92	85.45
7f	3.711	1.00	-1.63	76.22
7g	3.116	1.00	0.12	76.22
7i	3.265	-0.92	-3.00	122.04
8f	3.865	0.90	-0.63	76.22
8h	3.367	0.09	-0.26	76.22
8i	3.681	-0.24	-2.44	122.04
Tolrestat	3.065	0.11	0.06	81.86

^a pK_a predictions refers to the carboxylic groups. ^b Calculated *n*-octanol/water partition coefficient. ^c Calculated distribution coefficient. ^d Topological polar surface area.

Pharmacological Evaluation of Compound 7c. The target of our research program was to disclose potent and selective ALR2 inhibitors as novel potential candidates for the topical treatment of diabetic visual impairments. We therefore tested the efficacy of the novel compounds in preventing nuclear cataract after administration as an eye-drop solution in the precorneal region of severely galactosemic rats. Topical application is, in fact, the best way of drug administration for the treatment of ocular diseases, as it makes it possible to achieve significant drug levels in the site of action, thus circumventing first-pass metabolism in the liver and avoiding undesirable side effects typical of systemic administration.³⁶ As stated in the Introduction, topically administered drugs must possess adequately balanced hydrophilic-lipophilic properties in order to accomplish an exhaustive ocular absorption. Thus, focusing on the most active *in vitro* inhibitors, namely **7c,f,g,i** and **8f,h,i**, we analyzed their key physicochemical properties in order to identify the best candidate for the *in vivo* assay. Table 3 lists pK_a, ClogP, ClogD, and TPSA data, which were calculated *in silico* as useful descriptors to estimate ionization, lipophilicity, and polarity, respectively, of the selected compounds.³⁷ For a proper comparison, the same values were calculated also for tolrestat, a carboxylic-type ALR2 inhibitor, which proved to prevent cataract development in severely galactosemic rats when topically administered through ocular instillation.³⁶ Derivative **7c**, showing the best inhibitory potency, turned out to be less ionized, more lipophilic, and fairly polar when compared to its analogues. Moreover, **7c** emerged also as less ionized, more lipophilic, and almost as polar as tolrestat, thus providing, among all compounds, the most promising data set for an adequate ocular uptake. Therefore, **7c** was administered as a 3% solution to young rats fed a 50% galactose diet, four times daily for 21 days, in order to verify its ability to prevent or, at least, delay, nuclear cataract development. Its effectiveness was evaluated with respect to tolrestat. The pharmacological data are reported in Table 4. At the end of the assay, 100% of galactosemic rats treated only with the vehicle developed nuclear cataracts, whereas an almost complete and significant protection was detected in rats treated with **7c**. No nuclear cataracts were developed by rats administered a 3% ophthalmic solution of tolrestat. Furthermore, a slit-lamp examination of rat lenses was performed to better evaluate the progression of opacification (Figure 1). Galactosemic animals treated with the vehicle showed a mature cataract (Figure 1a), while up to 80% of the animals treated with **7c** developed widespread small vacuoles in the equatorial area, attaining stage 2 of lens opacity as graded by Kador et al.³⁸ (Figure 1b). The same was also true for all the animals administered with tolrestat, whose lenses, reported in Figure 1c, showed only slight changes with respect to lenses from animals on a normal diet, administered with the vehicle, which remained clear throughout the assay (Figure 1d).

Table 4. Effects of Treatment with Ophthalmic Solution of **7c** and Tolrestat on Development of Nuclear Cataract in Severely Galactosemic Rats

day of treatment	rats with nuclear cataract		
	control	7c (3%)	Tolrestat (3%)
11	13	0	0
12	25	0	0
13	25	0	0
14	25	0	0
15	25	0	0
16	31	0	0
17	50	0	0
18	65	0	0
19	80	13	0
20	92	13	0
21	100	20	0

Thus, the novel five-membered ARI **7c** proved to be not only a potent and selective inhibitor but also an excellent drug candidate for the topical treatment of ocular diseases.

Docking Studies. A three-dimensional comparison of the available aldose reductase-inhibitor X-ray complexes underlines the fact that ALR2 has a fairly flexible binding site able to change its shape with respect to the different inhibitors bound. In particular, the most striking difference resides in a pocket named the “specificity pocket”, which can be closed, as in the case of sorbinil, or open, as in the case of IDD594, tolrestat, or zopolrestat. The matter is further complicated by the fact that the degree and the mode of the pocket opening is inhibitor-dependent, e.g., in the case of tolrestat, the opening of the specificity pocket is perpendicular to that of IDD594. Very recently, it has been demonstrated that neither classic molecular dynamics simulations nor the currently available flexible docking approach are really able to predict such rearrangements upon ligand binding and that the Glide docking program, which performs a sort of “induced-fit docking”, did not succeed in obtaining better binding modes with respect to other docking programs such as Autodock, which fits the inhibitor into a rigid enzyme conformation.²⁷ As a result, it seems that, to date, the best approach aimed to find reliable binding modes for the ALR2 inhibitors is to consider multiple ALR2 binding conformations in the docking process.

For this reason, compound **7c**, the most active in the series, was docked by means of the Autodock program into the three main binding conformations of ALR2, best represented by the complexes with sorbinil (PDB code: 1AH0³⁹), tolrestat (PDB code: 2FDZ⁴⁰), and IDD594 (PDB code: 1US0⁴¹). Among the different docking programs, Autodock was chosen for our studies as it had already been effectively employed also in searching for the most favorable ALR2 conformation to host a given inhibitor²⁷ and it had been successfully used in scoring the different binding conformations of ALR2 inhibitors.³¹

Regarding the docking of **7c** in 1AH0, although the calculation converged toward one highly populated cluster (40 times out of 50, ΔG of binding = -7.0 kcal/mol), it did not succeed in providing reliable binding modes, as for all the proposed solutions, the anion-binding pocket is filled by the phenyl ring, while the carboxylate group points toward the solvent and interacts with Met301 and/or Ser302 backbone NH, in contrast with the experimentally observed binding modes for almost all other carboxylate-type inhibitors. As a consequence, 1AH0 was not considered for further docking studies on our compounds.

On the other hand, better results, although not completely convincing, were obtained when 2FZD was used as the possible

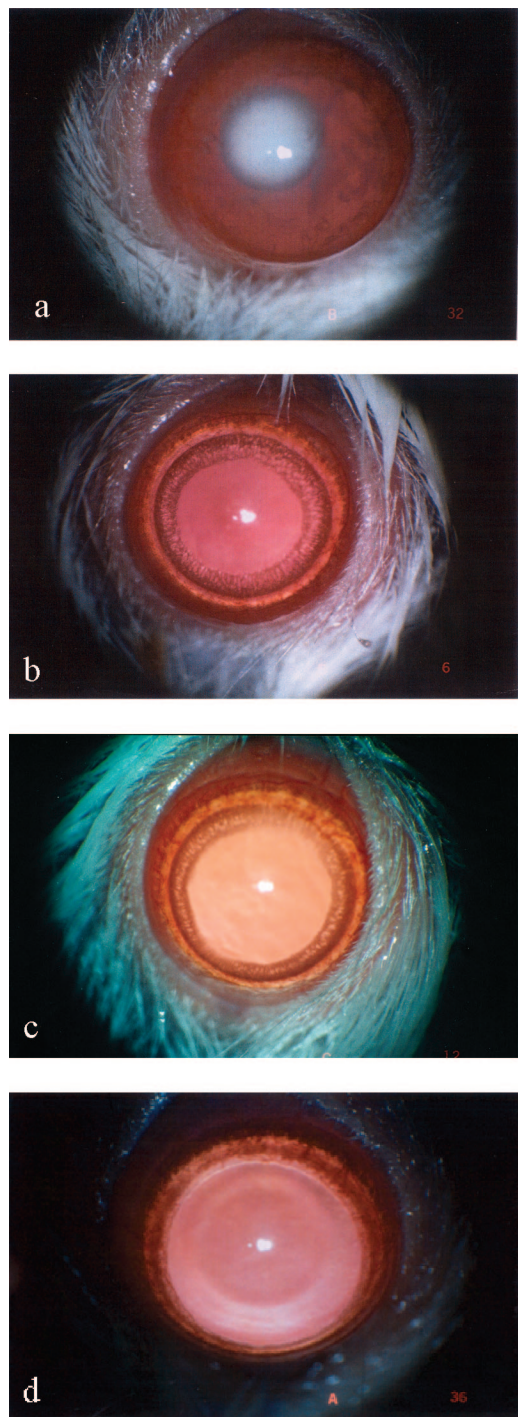


Figure 1. Slit-lamp evaluation of cataract formation in severely galactosemic rats after 21 days of treatment with test compounds **7c** and tolrestat. Image (a) shows lenses of galactosemic control rats administered only the vehicle. Image (b) shows lenses of galactosemic rats treated with **7c** at 3%. Image (c) shows lenses of galactosemic rats treated with tolrestat at 3%. Image (d) shows lenses of non-galactosemic control rats administered only the vehicle.

conformation. Indeed, the most highly populated family (ΔG of binding = -6.6 kcal/mol found 13 times out of 50) has the inhibitor carboxylate group anchored in the anion-binding pocket through two hydrogen bonds, with Tyr48 OH and His110 N^{ε2}H, and an electrostatic interaction with the nicotinamide moiety of the cofactor NADP⁺. However, the *para*-methoxy phenyl ring is not deeply fitted into the “specificity pocket”, as it is supposed to be from the experimental data, but remains partially

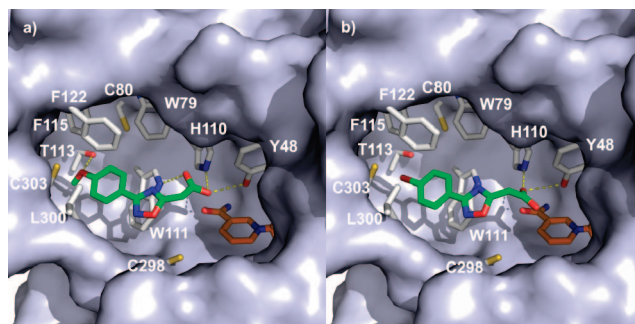


Figure 2. Stick representation of (a) compound **7c** (green) and (b) **7f** (green) bound into the active site of ALR2 shown as light-blue Connolly surface. The NADP⁺ is represented with its carbon atoms colored in orange. ALR2 residues relevant for inhibitor binding have been labelled, and their side chains are shown as white sticks. Nonpolar hydrogens have been removed for clarity reasons. Hydrogen bonds are displayed as yellow dashed lines.

solvent-exposed. Therefore, this binding mode does not fully agree with all the SARs developed concerning the phenyl ring.

Docking calculations using the IDD594-bound conformation (PDB code: 1US0) definitely showed the best results. Indeed, docking calculations of compound **7c** clearly converged to one binding mode (31 out of 50 runs, $\Delta G = -8.5$ kcal/mol), consistent both with the known carboxylate-type inhibitor binding modes and the SAR studies observed for series **7**. Moreover, docking of **7c** into the IDD594-bound conformation resulted in a better energy score, which is more in line with the experimentally tested inhibitory activity. The inhibitor is tightly anchored in the anion-binding pocket, with its carboxylate function involved in an electrostatic interaction with the positively charged nicotinamide moiety of the cofactor NADP⁺, and a network of H-bonds with Tyr48 OH, His110 N^{ε2}H, and Trp111 N^{ε1}H (Figure 2a). The phenyl ring of **7c** gets tightly trapped in the hydrophobic cage of the “specificity pocket” formed by Trp79, Trp111, Phe115, Phe122, and Leu300, performing aromatic and hydrophobic interactions with Phe115, Phe122, Trp79, and Leu300 and a parallel π - π interaction with the Trp111 side chain with a distance of 3.7 Å between the two aromatic planes.

The oxygen of the methoxy group was hydrogen-bonded to the Thr113 OH (the distance between the two oxygens is 3.2 Å), while the methyl group formed van der Waals contacts with the Thr113 C^γ and the Cys303 C^β (distances are 3.1 and 3.2 Å, respectively). These latter two interactions would explain the difference in activity observed between **7b** and **7c** and **7a** and **7b**, respectively.

Regarding the oxadiazole spacer of **7c**, although the oxygen of the ring was not found to be involved in any direct H-bond with the surrounding residues, due to its withdrawing property, it certainly improves stacking interactions with electron-rich rings such as the indole moiety of Trp111. However, we have to note the close proximity of the oxygen atom to the Cys298 SH group (≈ 3 Å), which, together with the known flexibility of the Val297–Leu300 region,^{31,42} would suggest a possible interaction.

As a result, our docking studies performed on **7c** indicate that, rather than the three main ALR2 conformations, the IDD594-bound structure is the most favorable to host our inhibitors. A superimposition of **7c** and IDD594 in their bound conformations (1US0 as receptor) shows that both compounds are firmly anchored in the active site through hydrogen bonds to His110, Tyr48, and Trp111 and establish a strong electrostatic interaction with NADP⁺. Moreover, both the inhibitors share

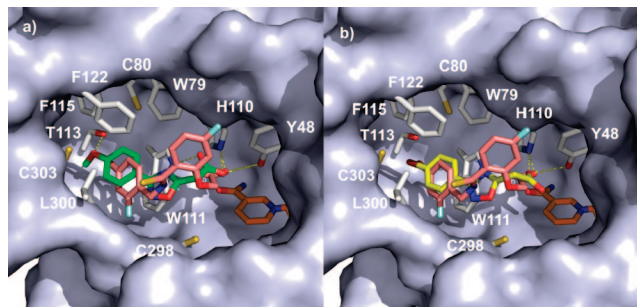


Figure 3. (a) Superimposition of the theoretical bound conformations of (a) **7c** (green), (b) **7f** (yellow), and the experimental bound conformation of IDD594 (pink) in the active site of ALR2 (PDB code: 1US0) shown as light-blue Connolly surface. The NADP⁺ is represented with its carbon atoms colored in orange. ALR2 residues relevant for inhibitor binding have been labelled, and their side chains are shown as white sticks. Nonpolar hydrogens have been removed for clarity reasons. Hydrogen bonds are displayed as yellow dashed lines.

the stacking between one of their aromatic rings and the Trp111 side chain and interact with the Thr113 side chain (Figure 3a).

The results of our docking experiments using compound **7c** as the ligand are perfectly in line with results of a virtual screening (VS) experiment performed by G. Klebe et al.³⁰ using the IDD594-bound conformation as the ALR2 structure. From this *in silico* screening, six new carboxylate-type leads were found and, interestingly, two of them, namely 4-[3-(3-nitrophenyl)-1,2,4-oxadiazol-5-yl]butanoic acid and 2-[5-(5-nitrofuranyl)-1,3,4-oxadiazol-2-yl-thio]acetic acid, share an overall similarity with ours. A crystallographic study of the complex between the 1,2,4-oxadiazole-containing inhibitor and ALR2 revealed the presence of an interstitial water molecule, mediating a hydrogen bond contact between the Trp111 N^ε1H and the carboxylic group of the inhibitor. On the basis of these results, we cannot exclude a priori the presence of a water molecule to mediate a similar contact in our 1,2,4-oxadiazole inhibitors, hence **7c** was also docked in the 1,2,4-oxadiazole-bound conformation of ALR2 taking into account such a water molecule (PDB code: 2IKG³¹). Docking results converged to one highly populated cluster of solutions (37 times out of 50, $\Delta G = -6.4$ kcal/mol), which showed that, while the carboxylate group of **7c** H-bonds with the water molecule mediating the contact with Trp111 N^ε1H, it is not close enough to interact with the Tyr48 and His110 side chains. As a consequence of the lack of these interactions, the ΔG of binding of the lowest energy conformation of the cluster is fairly high ($\Delta G = -6.4$ kcal/mol) and considerably worse than that calculated when the docking of **7c** was performed using 1US0 as the receptor ($\Delta G = -8.5$ kcal/mol). Thus, the presence of such a water molecule seemed unlikely in the case of our inhibitors, and consequently the docking of **7f**, **7i**, **8a**, and **8h** was subsequently performed using the IDD-bound ALR2 conformation (1US0).

The molecular docking calculations of **7f** converged toward one single cluster of solutions, where the inhibitor was involved in hydrogen bonds with Tyr48 OH and His110 N^ε2H and electrostatic interactions with the positively charged nicotinamide moiety of the cofactor (Figure 2b). The polarizable bromine atom is lodged at the tip of the hydrophobic pocket and proved to be quite close to Thr113 ≈ 3.2 Å. Interestingly, the position of this deeply buried bromine atom is spatially equivalent to that occupied by the bromine atom present in zenarestat and in IDD594 (Figure 3b).

The SAR studies clearly indicate that, among the compounds sharing a halogen in the para position on the phenyl ring, the

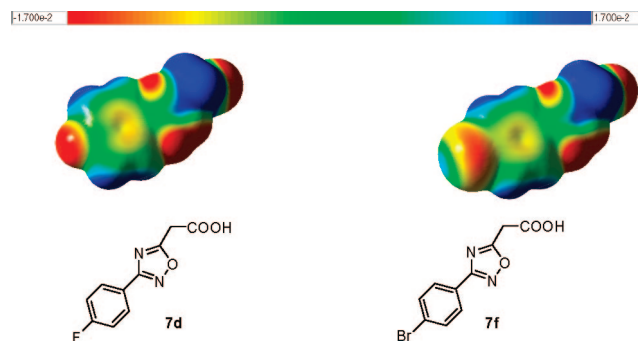


Figure 4. Electrostatic potential of compound **7d** and **7f** computed using B3LYP and 6-31G* basis set with a scale of -0.017 (red) to 0.017 hartree (blue).

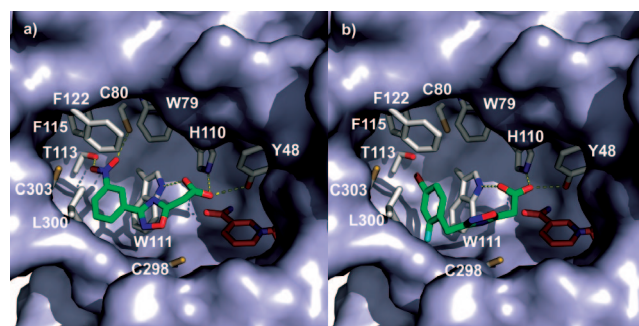


Figure 5. Stick representation of (a) compound **7i** (green) and (b) **8h** (green) bound into the active site of ALR2 shown as light-blue Connolly surface. The NADP⁺ is represented with its carbon atoms colored in orange. ALR2 residues relevant for inhibitor binding have been labelled, and their side chains are shown as white sticks. Nonpolar hydrogens have been removed for clarity reasons. Hydrogen bonds are displayed as yellow dashed lines.

one with the bromine atom gave the best IC₅₀ value (see compounds **7d**, **7e**, and **7f** in Table 1). With the aim of rationalizing these SAR data and to get an insight into the electrostatic potential profile of these compounds, we performed some *ab initio* calculations mapping the electrostatic potential of **7d** and **7f** onto the molecular surfaces representing the respective electron densities (Figure 4). While the fluorine atom, due to its small atomic radius, is entirely electronegative and consequently unable to engage in an interaction with an oxygen atom lone pair, the larger bromine shows the emergence of an electropositive crown, giving rise to a charge-transfer interaction with the electron pairs of the Thr113 O^γ. Regarding **7e**, molecular electrostatic potential calculations revealed a reduced size and intensity of the electropositive crown for the chlorine atom, compared with that of bromine; this is perfectly in line with the observation that **7e** has an IC₅₀ lower than **7d** but higher than **7f**. Thus, the most favorable activity of **7f**, if compared with **7d** and **7e**, can be attributed to the better halogen–oxygen lone pair interaction established with Thr113 O^γ.

Regarding compound **7i**, it exhibits a submicromolar IC₅₀ (0.71 μM) and docking calculations converged to one single cluster of solutions. The hydrogen bonds with Tyr48 OH, His110 N^ε2H, and Trp111 N^ε1H were all maintained, as well as the electrostatic interaction with the nicotinamide moiety of the NADP⁺ cofactor. The phenyl ring occupied the specificity pocket stacked between the Trp111 and Leu300 side chains, with the nitro group anchored to the upper part of this pocket through two hydrogen bonds with the Cys80 and Thr113 side chains (Figure 5a). However, it has to be said that, according to the previously mentioned X-ray analysis³¹ of the butanoic

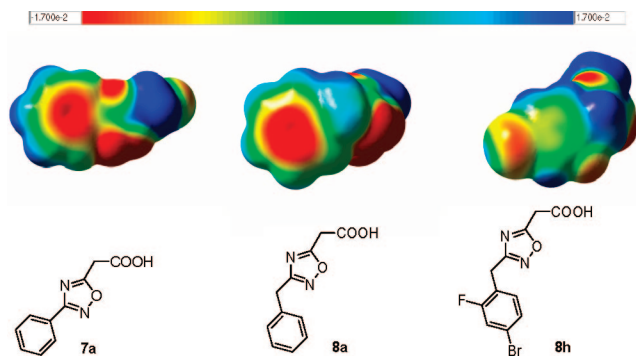


Figure 6. Electrostatic potential of compounds **7a**, **8a**, and **8h** computed using B3LYP and 6-31G* basis set with a scale of -0.017 (red) to 0.017 kcal mol $^{-1}$ (blue).

acid inhibitor containing the 1,2,4-oxadiazole core structure, the presence of the *meta*-nitro substituent is able to induce a flip of the Ala299–Leu300 backbone, thus establishing a hydrogen bond between one of the ligand's nitro oxygens and the Leu300 backbone NH (PDB code of the complex: 2IKG). Moreover, a small rotation of the χ_1 of Tyr309 making room for the nitro group was also observed, allowing a “nonclassical hydrogen bond” of the nitro oxygen with the C $^{\delta 1}$ H and C $^{\epsilon 1}$ H of Tyr309. These two structural variations with respect to the 1US0 structure seem to be typical of the nitro-containing inhibitors, as compounds possessing a weaker hydrogen bond acceptor such as a fluorine atom in the corresponding position were not able to induce a similar enzyme rearrangement. Thus, just for compound **7i**, with the aim of obtaining further insight into the positioning of the nitro group, docking calculations were also performed using 2IKG as the receptor. Surprisingly, even if the lowest energy cluster ($\Delta G = -7.7$ kcal/mol) was not highly populated (8 out of 50 runs), it showed a binding mode perfectly superimposable on that obtained using 1US0 as the referring model. By contrast, the most populated cluster (25 out of 50 runs) clearly showed the nitro group bound to the Leu300 backbone NH group, but the main interactions with Tyr48 OH, His110 N $^{\epsilon 2}$ H, and Trp111 N $^{\epsilon 1}$ H were completely lost, thus leading to a higher ΔG value (-6.5 kcal/mol). In conclusion, the docking calculations on **7i** would lead one to think that the nitro group binds to the upper part of the specificity pocket, although the other hypothesis cannot be excluded a priori due to a possible rearrangement of the enzyme upon ligand binding. On the basis of these results, in prospect it would be worth inserting two hydrogen bond acceptors in both of the *meta* positions of the phenyl ring of **7i** with the aim of simultaneously binding the upper and the lower part of the specificity pocket.

Compounds **8a–i**, which possess a methylene bridge connecting the phenyl and the oxadiazole rings, are generally less potent inhibitors than their analogues **7a–i**. Docking of **8a** and **8h** into the ALR2 active site shows that their binding mode does not substantially diverge from that observed for **7c**, **7f**, and **7i**. However, due to the presence of a methylene group, compounds **8a–i** have a different shape and mostly different electron properties with respect to compounds **7a–i**. For example, regarding **8a**, the electron-donating property of the methylene spacer results in a more negative value of the electrostatic potential on the phenyl ring (Figure 6) compared with compound **7a**, and this negatively affects the interaction with the electron-rich indole ring of Trp111. This finding can be extended to all the other methylene-containing compounds, resulting in a general lowering of their inhibitory activity. The particularly low activity of **8a** is likely to be determined also

Table 5. Results of 50 Independent Docking Runs for Each Inhibitor Using the ALR2/IDD594-Bound Conformation (1US0)

N	N_{tot}^a	f_{occ}^b	$\Delta G_{\text{binding}}^c$	T- K_i^d	IC $_{50}^e$
7c	7	31	-8.5	546	270
7f	1	50	-6.9	8500	690
7i	1	50	-8.4	690	710
8a	14	18	-8.2	1000	28400
8h	6	37	-8.4	696	360

^a N_{tot} is the total number of clusters. ^b f_{occ} is the frequency of occurrence and it represents the number of results in the chosen cluster (see Experimental Section). ^c $\Delta G_{\text{binding}}$ is the estimated free energy of binding of the chosen cluster and is given in kcal/mol. ^d T- K_i is the theoretical K_i predicted by the AutoDock program, and it is expressed in nM. ^e IC $_{50}$ is expressed in nM and it refers to the experimentally determined IC $_{50}$ reported in Table 1.

by the absence of substituents on the benzyl ring capable of establishing any favorable contact with the enzyme.

Accordingly, inhibitor **8h**, bearing an *ortho*-fluoro, *para*-bromo phenyl ring, shows a more positive electrostatic potential on the aryl ring, compared with all the other inhibitors (Figure 6). Thus, the low IC $_{50}$ observed for **8h** can be ascribed to the strengthening both of π – π interaction with the Trp111 side chain on one hand and of the bromine short contact with Thr113 O $^{\gamma}$ lone pair on the other. Moreover, docking of **8h** into the active site shows that the fluorine atom in the *ortho* position would establish a polar interaction with the Tyr309 hydroxyl group (Figure 5b).

It has to be said that, for all docking calculations, the new version of the AutoDock program (version 4.0) was used. The latest version of this software implements a novel force field, which, using an improved thermodynamic model of the binding process, allows inclusion of intramolecular terms in the estimated free energy of binding. Moreover, the new force field includes a full desolvation model that contains terms for all atom types. Unlike the previous version, AutoDock 4 computes, considering the desolvation energy term, the internal energy of the unbound state of the ligand before docking, and includes the difference of the internal energy between this unbound state and the final docked state when estimating the free energy of binding. Thus, all these changes are expected to result in an improved prediction of the free energy of binding and thus of the inhibition constant K_i associated with a given binding mode.

It is known that for a competitive inhibitor a linear correlation between K_i and IC $_{50}$ exists:

$$\text{IC}_{50} = K_i(1 + S/K_m)$$

where S and K_m are the substrate concentration and the Michaelis–Menten constant of the substrate, respectively.⁴³ Because S and K_m are both constant, seeing that the assays are performed under the same conditions, a direct comparison between the K_i values calculated by AutoDock and the experimental IC $_{50}$ is feasible. Looking at Table 5, it emerges that, as a general rule, the estimated K_i reproduces reasonably well the experimental inhibition data. In fact, the predicted K_i of **7c**, **7i**, and **8h** are in the nanomolar range, in accordance with the experimental IC $_{50}$. Also for compound **8a**, both the experimental IC $_{50}$ and the predicted K_i are in the micromolar range. Moreover, **7c**, which is the most active inhibitor of the series, has the lowest K_i . According to the IC $_{50}$ values, compound **8a**, compared with **7c**, **7i**, and **8h**, is considerably less active and correspondingly it has a higher K_i . By contrast, **7f** is the only compound that has a considerable discrepancy between the predicted and the experimental activity. Indeed, **7f** was predicted to be less active than it really is and this could be probably due to the peculiar electrostatic properties of the

bromine atom, which are not accurately taken into account by the docking scoring function. However, when the Lamarckian genetic algorithm is used as a search method, the f_{occ} (Table 5), which for **7f** is the best possible, is an important indication of the goodness of the compound.

To sum up, through an ensemble docking approach, we defined first the most favorable ALR2 binding conformation for our inhibitors. The presence of an interstitial water molecule mediating the contact with Trp111 seemed unlikely, and the binding modes of our compounds were defined. The proposed modes of binding of our inhibitors are perfectly in line with the SARs here observed, and with the exception of **7f**, the predicted K_i are in line with the experimental IC_{50} s observed. The knowledge of the structure of the binding site together with an understanding of the binding mode of our compounds provides the platform for further structure-guided design hypotheses of novel drug candidates with a higher affinity and selectivity.

Experimental Section

Chemistry. Melting points were determined using a Reichert Köfler hot-stage apparatus and are uncorrected. Infrared spectra were recorded with a FT-IR spectrometer Nicolet/Avatar in Nujol mulls. Routine nuclear magnetic resonance spectra were recorded in DMSO- d_6 solution on a Varian Gemini 200 spectrometer operating at 200 MHz. Mass spectra were obtained on a Hewlett-Packard 5988 A spectrometer using a direct injection probe and an electron beam energy of 70 eV. Evaporation was performed in vacuo (rotary evaporator). Analytical TLCs were carried out on Merck 0.2 mm precoated silica gel aluminum sheets (60 F-254). Silica gel column chromatographies were performed with Merck Silica gel 60 (230–400 mesh ASTM). Elemental analyses were performed by our Analytical Laboratory and agreed with theoretical values to within $\pm 0.4\%$.

Benzonitrile, 4-methylbenzonitrile, 4-methoxybenzonitrile, 4-fluorobenzonitrile, 4-chlorobenzonitrile, 4-bromobenzonitrile, 4-trifluoromethylbenzonitrile, 4-bromo-2-fluorobenzonitrile, 3-nitrobenzonitrile, 2-phenylacetoneitrile, 2-*p*-tolylacetoneitrile, 2-(4-methoxyphenyl)acetoneitrile, 2-(4-fluorophenyl)acetoneitrile, 2-(4-bromophenyl)acetoneitrile, 2-(4-chlorophenyl)acetoneitrile, 2-(4-bromo-2-fluorophenyl)acetoneitrile, 2-(3-nitro-phenyl)acetoneitrile, benzamide, 4-methylbenzamide, 4-methoxybenzamide, 4-fluorobenzamide, ethyl 3-chloro-3-oxopropanoate, and ethyl 4-chloro-3-oxobutanoate used to obtain the target inhibitors were from Sigma-Aldrich and Fluka.

General Procedure for the Synthesis of *N*-Hydroxybenzimidamides **3a–i and *N*-Hydroxy-2-phenylacetimidamides **4a–i**.** A solution of the appropriate nitrile **1a–i** or **2a–i** (1.00 mmol), hydroxylamine hydrochloride (1.35 mmol), and potassium carbonate (1.00 mmol) in ethanol was left under stirring at room temperature for 1 h, then heated under reflux until the disappearance of the starting materials (6 h, TLC analysis). After cooling, the resulting mixture was filtered and the solvent was evaporated to dryness under reduced pressure to give the target compound as a white solid, which was purified by recrystallization (Supporting Information, Tables 1 and 2).

General Procedure for the Synthesis of Ethyl 2-(3-Phenyl-1,2,4-oxadiazol-5-yl)acetates **5a–i and Ethyl 2-(3-Benzyl-1,2,4-oxadiazol-5-yl)acetates **6a–i**.** Sodium hydride (1.00 mmol, 60% dispersion in mineral oil) was added portionwise, under a nitrogen atmosphere, to an ice-cooled solution of the appropriate *N*-hydroxybenzimidamide **3a–i** (1.00 mmol), or *N*-hydroxy-2-phenylacetimidamide **4a–i** (1.00 mmol), in dry toluene. Once addition was complete, the mixture was left under stirring at room temperature for 1 h. Then, ethyl 3-chloro-3-oxopropanoate (1.00 mmol) was added dropwise, under stirring and with cooling, and the resulting suspension was heated under reflux until disappearance of the starting materials (18–24 h, TLC analysis). After cooling, the reaction mixture was filtered and the solvent was evaporated to dryness under reduced pressure to the desired ester, which was

purified by recrystallization. When obtained as oily products, the title compounds were purified by silica gel column chromatography using petroleum ether 60–80 °C/AcOEt 9/1 as the eluent (Supporting Information, Tables 3 and 4).

General Procedure for the Synthesis of 2-(3-Phenyl-1,2,4-oxadiazol-5-yl)acetic Acids **7a–i and 2-(3-Benzyl-1,2,4-oxadiazol-5-yl)acetic Acids **8a–i**.** A suspension of the appropriate ester derivative **5a–i** or **6a–i** (1.00 mmol) in 5 mL of aqueous sodium hydroxide 1N was heated under stirring at 110 °C until hydrolysis was complete (1 h, TLC analysis). After cooling, the reaction mixture was acidified with hydrochloric acid 1 M under ice-cooling. The white solid separated was collected and purified by recrystallization (Supporting Information, Tables 5 and 6).

General Procedure for the Synthesis of Ethyl 2-(2-Phenyl-oxazol-4-yl)acetates **10a–d.** A mixture of the appropriate benzamide (1.00 mmol) and ethyl 4-chloro-3-oxobutanoate (1.00 mmol) was heated at 125 °C under stirring until the disappearance of the starting material (1 h, TLC analysis). After cooling, the resulting mass was diluted with saturated sodium bicarbonate, then extracted with cyclohexane. The combined extracts were dried with magnesium sulfate, filtered, and evaporated to dryness to the desired ester, which was purified by recrystallization. When obtained as oily products, the title compounds were purified by silica gel column chromatography using petroleum ether 60–80 °C/AcOEt 9/1 as the eluent (Supporting Information, Table 7).

General Procedure for the Synthesis of 2-(2-Phenyl-oxazol-4-yl)acetic Acids **11a–d.** A suspension of the appropriate ester **10a–d** (1.00 mmol) in 5 mL of aqueous sodium hydroxide 1N was heated at reflux under stirring until hydrolysis was complete (1 h, TLC analysis). The reaction mixture was cooled to room temperature and then acidified with hydrochloric acid 1M under ice-cooling. The white solid precipitated was collected, washed with water, and purified by recrystallization (Supporting Information, Tables 8 and 9).

Biology. Materials and Methods. Aldose reductase (ALR2) and aldehyde reductase (ALR1) were obtained from Sprague–Dawley albino rats, 120–140 g body weight, supplied by Harlan Nossan, Italy. To minimize cross-contamination between ALR2 and ALR1 in the enzyme preparation, rat lens, in which ALR2 is the predominant enzyme, and kidney, where ALR1 shows the highest concentration, were used for the isolation of ALR2 and ALR1, respectively.

Pyridine coenzyme, D,L-glyceraldehyde, and sodium D-glucuronate were from Sigma-Aldrich. Tolrestat was obtained from Lorestat Recordati, Italy. All other chemicals were of reagent grade.

Enzyme Preparation. Aldose Reductase (ALR2). A purified rat lens extract was prepared in accordance with the method of Hayman and Kinoshita⁴⁴ with slight modifications. Lenses were quickly removed from rats following euthanasia and were homogenized (Glas-Potter) in 3 volumes of cold deionized water. The homogenate was centrifuged at 12000 rpm at 0–4 °C for 30 min. Saturated ammonium sulfate solution was added to the supernatant fraction to form a 40% solution, which was stirred for 30 min at 0–4 °C and then centrifuged at 12000 rpm for 15 min. Following this same procedure, the recovered supernatant was subsequently fractionated with saturated ammonium sulfate solution using first a 50% and then a 75% salt saturation. The precipitate recovered from the 75% saturated fraction, possessing ALR2 activity, was redissolved in 0.05 M NaCl and dialyzed overnight in 0.05 M NaCl. The dialyzed material was used for the enzymatic assay.

Aldehyde Reductase (ALR1). Rat kidney ALR1 was prepared in accordance with a previously reported method.³³ Kidneys were quickly removed from normal killed rats and homogenized (Glas-Potter) in 3 volumes of 10 mM sodium phosphate buffer, pH 7.2, containing 0.25 M sucrose, 2.0 mM EDTA dipotassium salt, and 2.5 mM β -mercaptoethanol. The homogenate was centrifuged at 12000 rpm at 0–4 °C for 30 min, and the supernatant was subjected to a 40–75% ammonium sulfate fractionation, following the same procedure previously described for ALR2. The precipitate obtained from the 75% ammonium sulfate saturation, possessing ALR1 activity, was redissolved in 50 volumes of 10 mM sodium phosphate

buffer, pH 7.2, containing 2.0 mM EDTA dipotassium salt and 2.0 mM β -mercaptoethanol, and was dialyzed overnight using the same buffer. The dialyzed material was used in the enzymatic assay.

Enzymatic Assays. The activity of the two test enzymes was determined spectrophotometrically by monitoring the change in absorbance at 340 nm, which is due to the oxidation of NADPH catalyzed by ALR2 and ALR1. The change in pyridine coenzyme concentration/min was determined using a Beckman DU-64 kinetics software program (Solf Pack TM Module).

ALR2 activity was assayed at 30 °C in a reaction mixture containing 0.25 mL of 10 mM D,L-glyceraldehyde, 0.25 mL of 0.104 mM NADPH, 0.25 mL of 0.1 M sodium phosphate buffer (pH 6.2), 0.1 mL of enzyme extract, and 0.15 mL of deionized water in a total volume of 1 mL. All the above reagents, except D,L-glyceraldehyde, were incubated at 30 °C for 10 min; the substrate was then added to start the reaction, which was monitored for 5 min. Enzyme activity was calibrated by diluting the enzymatic solution in order to obtain an average reaction rate of 0.011 \pm 0.0010 absorbance units/min for the sample.

ALR1 activity was determined at 37 °C in a reaction mixture containing 0.25 mL of 20 mM sodium D-glucuronate, 0.25 mL of 0.12 mM NADPH, 0.25 mL of dialyzed enzymatic solution, and 0.25 mL of 0.1 M sodium phosphate buffer (pH 7.2) in a total volume of 1 mL. The enzyme activity was calibrated by diluting the dialyzed enzymatic solution in order to obtain an average reaction rate of 0.015 \pm 0.0010 absorbance/min for the sample.

Enzymatic Inhibition. The inhibitory activity of the newly synthesized compounds against ALR2 and ALR1 was assayed by adding 0.1 mL of the inhibitor solution to the reaction mixture described above. All the inhibitors were solubilized in water and the solubility was facilitated by adjustment to a favorable pH. After complete solution, the pH was readjusted to 7. To correct for the nonenzymatic oxidation of NADPH and for absorption by the compounds tested, a reference blank containing all the above assay components except the substrate was prepared. The inhibitory effect of the new derivatives was routinely estimated at a concentration of 10⁻⁴ M. Those compounds found to be active were tested at additional concentrations between 10⁻⁵ and 10⁻⁸ M. The determination of the IC₅₀ values was performed by linear regression analysis of the log-dose response curve, which was generated using at least four concentrations of the inhibitor, causing an inhibition between 20% and 80%, with two replicates at each concentration. The 95% confidence limits (95% CL) were calculated from *t* values for *n* - 2, where *n* is the total number of determinations.

Pharmacology. Materials and Methods. Experiments were carried out using Sprague-Dawley albino rats, 45–55 g body weight, supplied by Harlan-Nossan, Italy. Animal care and treatment conformed to the ARVO Resolution on the Use of Animals in Ophthalmic and Vision Research. The galactose diet consisted of a pulverized mixture of 50% D-galactose and 50% TRM laboratory chow (Harlan Teckland UK), and the control diet consisted of normal TRM. Both control and experimental rats had access to food and water ad libitum.

Prevention of Cataract Development. The assay was performed following previously reported procedures, with slight modifications.^{45–47} Animals were randomly divided into four groups of equal average body weight with 15 rats per group. The test compound **7c** and the reference compound tolrestat were administered four times daily as 3% eye-drops in both eyes. The vehicle in which compounds were contained were administered with the same dose regimen to the control group, which was given access to the galactose diet, and to a group fed with a normal diet, which was included to record the aspect of normal lenses. The groups treated with the tested compounds were pre-dosed one day before switching their diet to the galactose-containing chow.

At the beginning of the experiment and after 6, 8, 10, 14, and 21 days of treatment, lenses were examined using slit-lamp microscopy after dilating the pupils with 1% atropine, Farmigea, Italy, to establish their integrity. The extent of lens opacity was graded as follows, according to the classification of Kador et al.:³⁸ stage 0, normal lens; stage 1, small vacuoles and/or tenuous radial

opacifications in the equatorial region; stage 2, peripheral vesicles and cortical opacities; stage 3, diffuse opacification involving the whole lens; stage 4, matured nuclear cataract readily visible as a white spot even to the naked eye. The number of animals that attained each stage was recorded and the significance of differences was analyzed using the Mann-Whitney U-test.

Computational Chemistry. Molecular Electrostatic Potential Calculations. For all compounds, the electrostatic potential was calculated by means of GAUSSIAN 03⁴⁸ and mapped onto the electron density surface for each compound. The isovalue of 0.0004 electron/Bhor³ was chosen for the definition of the density surface, while the electrostatic potential was computed using B3LYP functional and 6-31G* basis set with a scale of -0.017 (red) to 0.017 hartree (blue), -10.5 and 10.5 kcal mol⁻¹, respectively.

Docking Simulations. Molecular docking of **7c**, **7f**, **7g**, **7i**, **8a**, and **8h** into the three-dimensional X-ray structures of ALR-2 (PDB codes: 1AH0, 2FZD, 1US0, 2IKG) was carried out using the AutoDock software package (version 4.0) as implemented through the graphic user interface AutoDockTools (ADT 1.4.6).^{49,50}

Ligands and Protein Setup. The structures of the inhibitors were first generated from the standard fragment library of the SYBYL software version 7.3.⁵¹ Geometry optimizations were achieved with the SYBYL/MAXIMIN2 minimizer by applying the BFGS (Broyden, Fletcher, Goldfarb, and Shanon) algorithm⁵² with a convergence criterion of 0.05 kcal/mol and employing the TRIPOS force field. Then the constructed compounds (**7c**, **7f**, **7g**, **7i**, **8a**, and **8h**) and ALR2 X-ray structures (PDB codes: 1AH0, 2FDZ, 1US0, 2IKG) were converted to AutoDock format files using ADT. The inhibitors were modeled in their deprotonated, negatively charged states, and partial atomic charges on atoms were calculated with the Gasteiger method as implemented in ADT. It has to be said that although the inhibition assays on our compounds were conducted on rat ALR2, we used human ALR2 crystal structure (1US0) to explain ligand activity. This is because the three-dimensional structure of rat ALR2 is still unknown. However, human and rat sequences of ALR2 share 84% identity (calculated through the Align program as implemented in the Workbench server (<http://workbench.sdsc.edu/>)) and all active-site residues, including those of the specificity pocket, are conserved between the two enzymes. The only exception is represented by the conservative mutation of Phe121 (human), which is a tyrosine in the rat, although this residue was not involved in our inhibitor binding in any of the dockings performed.

Docking Setup. The docking area was defined by a box, centered on the C α of the Tpr111 residue. Grid points of 60 \times 60 \times 60 with 0.375 Å spacing were calculated around the docking area for all the ligand atom types using AutoGrid4. For each ligand, 50 separate docking calculations were performed. Each docking calculation consisted of 1 \times 10⁶ energy evaluations using the Lamarckian genetic algorithm local search (GALS) method. A low-frequency local search in accordance with the method of Solis and Wets was applied to docking trials to ensure that the final solution represents a local minimum. Each docking run was performed with a population size of 150, and 300 rounds of Solis and Wets local search were applied, with a probability of 0.06. A mutation rate of 0.02 and a crossover rate of 0.8 were used to generate new docking trials for subsequent generations. The GALS method evaluates a population of possible docking solutions and propagates the most successful individuals from each generation into the next one. The docking results from each of the 50 calculations were clustered on the basis of root-mean square deviation (rmsd = 1 Å) between the Cartesian coordinates of the ligand atoms and were ranked on the basis of the free energy of binding. For compounds **7c**, **7f**, and **7i**, the most highly populated family and that possessing the lowest energy of binding coincide, and within this family, the binding mode which presents the higher number of interactions with the enzyme is described in the Results and Discussion Section. For compounds **8a** and **8h**, the family which is the most highly populated, was considered and was described as more in agreement with SAR data with respect to the lowest-energy family.

Energy Refinement of Ligand/ALR2 Complexes. Refinement of the predicted ligand/ALR2 Complexes was achieved through energy minimizations using the TRIPOS force field as implemented in the SYBYL package. These geometric optimizations included 3000 steps of a steepest descent minimization, followed by 2000 steps of conjugate gradient minimization, keeping the backbone atoms fixed and protein side chains and the ligand free to move.

Supporting Information Available: Tables 1–10 including physical, spectral, and analytical data of compounds described. This material is available free of charge via the Internet at <http://pubs.acs.org>.

References

- (1) Kador, P. F. The Role of Aldose Reductase in the Development of Diabetic Complications. *Med. Res. Rev.* **1998**, *8*, 325–352.
- (2) Yabe-Nishimura, C. Aldose Reductase in Glucose Toxicity: a Potential Target for the Prevention of Diabetic Complications. *Pharmacol. Rev.* **1998**, *50*, 21–33.
- (3) Brownlee, M. Biochemistry and Molecular Cell Biology of Diabetic Complications. *Nature* **2001**, *414*, 813–820.
- (4) Altan, V. M. The Pharmacology of Diabetic Complications. *Curr. Med. Chem.* **2003**, *10*, 1317–1327.
- (5) Chung, S. S.; Chung, S. K. Genetic Analysis of Aldose Reductase in Diabetic Complications. *Curr. Med. Chem.* **2003**, *10*, 1375–1387.
- (6) Williamson, J. R.; Chang, K.; Frangos, M.; Hasan, K. S.; Ido, Y.; Kawamura, T.; Nyengaard, J. R.; van der Enden, M.; Kilo, C.; Tilton, R. G. Hyperglycemic Pseudohypoxia and Diabetic Complications. *Diabetes* **1993**, *42*, 801–813.
- (7) Ido, Y.; Williamson, J. R. Hyperglycemic Cytosolic Reductive Stress “Pseudohypoxia”: Implications for Diabetic Retinopathy. *Invest. Ophthalmol. Vis. Sci.* **1997**, *38*, 1467–1470.
- (8) Purves, T.; Middlemas, A.; Agthon, S.; Jude, E. B.; Boulton, A. J.; Fernyhough, P.; Tomlinson, D. R. A Role for Mitogen-Activated Protein Kinases in the Etiology of Diabetic Neuropathy. *FASEB J.* **2001**, *15*, 2508–2514.
- (9) Obrosova, I. G.; Li, F.; Abatan, O. I.; Forsell, M. A.; Komjati, K.; Pacher, P.; Szabo, C.; Stevens, M. J. Role of Poly(ADP-ribose)polymerase Activation in Diabetic Neuropathy. *Diabetes* **2004**, *53*, 711–720.
- (10) Jousen, A. M.; Poulaki, V.; Le, M. L.; Koizumi, K.; Esser, C.; Janicki, H.; Scharaermeyer, U.; Kociok, N.; Fauser, S.; Kirchof, B.; Kern, T. S.; Adamis, A. P. A Central Role for Inflammation in the Pathogenesis of Diabetic Retinopathy. *FASEB J.* **2004**, *18*, 1450–1452.
- (11) Sarges, R.; Oates, P. J. Aldose Reductase Inhibitors: Recent Developments. *Prog. Drug Res.* **1993**, *40*, 99–161.
- (12) Suzen, S.; Buyukbingol, E. Recent Studies of Aldose Reductase Enzyme Inhibition for Diabetic Complications. *Curr. Med. Chem.* **2003**, *10*, 1329–1352.
- (13) Kawanishi, K.; Ueda, H.; Moriyasu, M. Aldose Reductase Inhibitors from Nature. *Curr. Med. Chem.* **2003**, *10*, 1329–1352.
- (14) Klebe, G.; Kraemer, O.; Sotriffer, C. Strategies for the Design of Inhibitors of Aldose Reductase, an Enzyme Showing Pronounced Induced Fit Adaptations. *Cell. Mol. Life Sci.* **2004**, *61*, 783–793.
- (15) Dixit, B. L.; Balendiran, G. K.; Watowich, S. J.; Srivastava, S.; Ramana, K. V.; Petrash, J. M.; Bhatnagar, A.; Srivastava, S. K. Kinetic and Structural Characterization of the Glutathione-Binding Site of Aldose Reductase. *J. Biol. Chem.* **2000**, *275*, 21587–21595.
- (16) Ramana, K. V.; Dixit, B. L.; Srivastava, S.; Balendiran, G. K.; Srivastava, S. K.; Bhatnagar, A. Selective Recognition of Glutathionylated Aldehydes by Aldose Reductase. *Biochemistry* **2000**, *39*, 12172–12180.
- (17) Srivastava, S. K.; Ramana, K. V.; Bhatnagar, A. Role of Aldose Reductase and Oxidative Damage in Diabetes and the Consequent Potential for Therapeutic Options. *Endocr. Rev.* **2005**, *26*, 380–392.
- (18) Bohren, K. M.; Bullock, B.; Wermuth, B.; Gabbay, K. H. The Aldo-Keto Reductase Superfamily. *J. Biol. Chem.* **1989**, *264*, 9547–9551.
- (19) Jez, J. M.; Bennett, M. J.; Schlegel, B. P.; Lewis, M.; Penning, T. M. Comparative Anatomy of the Aldo-Keto Reductase Superfamily. *Biochem. J.* **1997**, *326*, 625–636.
- (20) El-Kabbani, O.; Wilson, D. K.; Petrash, J. M.; Quioco, F. A. Structural Features of the Aldose Reductase and Aldehyde Reductase Inhibitor-Binding Sites. *Mol. Vis.* **1998**, *4*, 19–25.
- (21) Petrash, J. M. All in the Family: Aldose Reductase and Closely Related Aldo-Keto Reductases. *Cell. Mol. Life Sci.* **2004**, *61*, 737–749.
- (22) Da Settimo, F.; Primofiore, G.; Da Settimo, A.; La Motta, C.; Taliani, S.; Simorini, F.; Novellino, E.; Greco, G.; Lavecchia, A.; Boldrini, E. [1,2,4]Triazino[4,3-*a*]benzimidazole Acetic Acid Derivatives: A New Series of Selective Aldose Reductase Inhibitors. *J. Med. Chem.* **2001**, *44*, 4359–4369.
- (23) Da Settimo, F.; Primofiore, G.; Da Settimo, A.; La Motta, C.; Simorini, F.; Novellino, E.; Greco, G.; Lavecchia, A.; Boldrini, E. Novel, Highly Potent Aldose Reductase Inhibitors: Cyano-(2-oxo-2,3-dihydroindol-3-yl)-acetic Acid Derivatives. *J. Med. Chem.* **2003**, *46*, 1419–1428.
- (24) Da Settimo, F.; Primofiore, G.; La Motta, C.; Salerno, S.; Novellino, E.; Greco, G.; Lavecchia, A.; Laneri, S.; Boldrini, E. Spirohydantoin Derivatives of Thiopyrano[2,3-*b*]pyridin-4(4*H*)-one as Potent in Vitro and in Vivo Aldose Reductase Inhibitors. *Bioorg. Med. Chem.* **2005**, *13*, 491–499.
- (25) Da Settimo, F.; Primofiore, G.; La Motta, C.; Sartini, S.; Taliani, S.; Simorini, F.; Marini, A. M.; Lavecchia, A.; Novellino, E.; Boldrini, E. Naphtho[1,2-*d*]isothiazole Acetic Acid Derivatives as a Novel Class of Selective Aldose Reductase Inhibitors. *J. Med. Chem.* **2005**, *48*, 6897–6907.
- (26) La Motta, C.; Sartini, S.; Mugnaini, L.; Simorini, F.; Taliani, S.; Salerno, S.; Marini, A. M.; Da Settimo, F.; Lavecchia, A.; Novellino, E.; Cantore, M.; Failli, P.; Ciuffi, M. Pyrido[1,2-*a*]pyrimidin-4-one Derivatives as a Novel Class of Selective Aldose Reductase Inhibitors Exhibiting Antioxidant Activity. *J. Med. Chem.* **2007**, *50*, 4917–4927.
- (27) Zentgraf, M.; Steuber, H.; Koch, C.; La Motta, C.; Sartini, S.; Sotriffer, C. A.; Klebe, G. How Reliable are Current Docking Approaches for Structure-Based Drug Design. *Angew. Chem., Int. Ed.* **2007**, *46*, 3575–3578.
- (28) Steuber, H.; Zentgraf, M.; La Motta, C.; Sartini, S.; Heine, A.; Klebe, G. Evidence for a Novel Binding Site Conformer of Aldose Reductase in Ligand Bound State. *J. Mol. Biol.* **2007**, *369*, 186–197.
- (29) Van Zandt, M. C.; Jones, M. L.; Gunn, D. E.; Geraci, L. S.; Jones, J. H.; Sawicki, D. R.; Sredy, J.; Jacot, J. L.; Dicioccio, A. T.; Petrova, T.; Mitschler, A.; Podjarny, A. D. Discovery of 3-[(4,5,7-trifluorobenzothiazol-2-yl)methyl]indole-*N*-acetic Acid (Lidorestat) and Congeners as Highly Potent and Selective Inhibitors of Aldose Reductase for Treatment of Chronic Diabetic Complications. *J. Med. Chem.* **2005**, *48*, 3141–3152.
- (30) Kraemer, O.; Hazemann, I.; Podjarny, A. D.; Klebe, G. Virtual Screening for Inhibitors of Human Aldose Reductase. *Proteins: Struct., Funct., Bioinf.* **2004**, *55*, 814–823.
- (31) Steuber, H.; Heine, A.; Klebe, G. Structural and Thermodynamic Study on Aldose Reductase: Nitro-substituted Inhibitors with Strong Enthalpic Binding Contribution. *J. Mol. Biol.* **2007**, *368*, 618–638.
- (32) Faul, M. M.; Winneroski, L. L.; York, J. S.; Reinhard, M. R.; Hoying, R. C.; Gritton, W. H.; Dominianni, S. J. Synthesis of 2-Phenylloxazole Derivatives Containing Amino Acids as Insulin Sensitivity Enhancers for Treatment of Type II Diabetes. *Heterocycles* **2001**, *55*, 689–704.
- (33) Ward, W. H. J.; Sennitt, C. M.; Ross, H.; Dingle, A.; Timms, D.; Mirrlees, D. J.; Tuffin, D. P. Ponalrestat: A Potent and Specific Inhibitor of Aldose Reductase. *Biochem. Pharmacol.* **1990**, *39*, 337–346.
- (34) Negro, T.; Murata, M.; Ueda, S.; Fujitani, B.; Ono, Y.; Kuromiya, A.; Komiya, M.; Suzuki, K.; Matsumoto, J. Novel, Highly Potent Aldose Reductase Inhibitors: (*R*)-(-)-2-(4-Bromo-2-fluorobenzyl)-1,2,3,4-tetrahydropyrrolo[1,2-*a*]pyrazine-4-spiro-3'-pyrrolidine-1,2',3,5'-tetrone (AS-3201) and its Congeners. *J. Med. Chem.* **1998**, *41*, 4118–4129.
- (35) Malamas, M. S.; Hohman, T. C.; Millen, J. Novel Spirosuccinimide Aldose Reductase Inhibitors Derived from Isoquinoline-1,3-diones: 2-[(4-Bromo-2-fluorophenyl)methyl]-6-fluorospiro[isoquinoline-4(1*H*),3'-pyrrolidine]-1,2',3,5'(2*H*)-tetrone and Congeners. 1. *J. Med. Chem.* **1994**, *37*, 2043–2058.
- (36) Banditelli, S.; Boldrini, E.; Vilardo, G. P.; Ceconi, I.; Cappiello, M.; Dal Monte, M.; Marini, I.; Del Corso, A.; Mura, U. A New Approach Against Sugar Cataract Through Aldose Reductase Inhibitors. *Exp. Eye Res.* **1999**, *69*, 533–538.
- (37) The pK_a , CLogP, CLogD calculations were performed with the chemsilico server on the web site: <http://chemsilico.com>. The TPSA calculation was performed with Marvin Sketch and Calculator Plugins on the web-Site: <http://www.chemaxon.com/demosite/marvin/index.html>.
- (38) Kador, P. F.; Akagi, Y.; Kinoshita, J. H. The Effect of Aldose Reductase and its Inhibition on Sugar Cataract Formation. *Metabolism* **1986**, *35*, 15–19.
- (39) Urzhumtsev, A.; Tete-Favier, F.; Mitschler, A.; Barbanton, J.; Barth, P.; Urzhumtseva, L.; Biellmann, J. F.; Podjarny, A.; Moras, D. A “Specificity” Pocket Inferred from the Crystal Structures of the Complexes of Aldose Reductase with the Pharmacologically Important Inhibitors Tolrestat and Sorbinil. *Structure* **1997**, *5*, 601–612.
- (40) Steuber, H.; Zentgraf, M.; Gerlach, C.; Sotriffer, C. A.; Heine, A.; Klebe, G. Expect the Unexpected or Caveat for Drug Designers: Multiple Structure Determinations Using Aldose Reductase Crystals Treated under Varying Soaking and Co-crystallisation Conditions. *J. Mol. Biol.* **2006**, *363*, 174–187.
- (41) Howard, E. I.; Sanishvili, R.; Cachau, R. E.; Mitschler, A.; Chevrier, B.; Barth, P.; Lamour, V.; Van Zandt, M.; Sibley, E.; Bon, C.; Moras,

- D.; Schneider, T. R.; Joachimiak, A.; Podjarny, A. Ultrahigh Resolution Drug Design I: Details of Interactions in Human Aldose Reductase–Inhibitor Complex at 0.66 Å. *Proteins* **2004**, *55*, 792–804.
- (42) Zentgraf, M.; Fokkens, J.; Sotriffer, C. A. Addressing Protein Flexibility and Ligand Selectivity by “in Situ Cross-Docking”. *ChemMedChem* **2006**, *1*, 1355–1359.
- (43) Cheng, Y.; Prusoff, W. H. Relationship Between the Inhibition Constant (K_i) and the Concentration of Inhibitor which Causes 50% Inhibition (IC_{50}) of an Enzymatic Reaction. *Biochem. Pharmacol.* **1973**, *22*, 3099–3108.
- (44) Hayman, S.; Kinoshita, J. H. Isolation and Properties of Lens Aldose Reductase. *J. Biol. Chem.* **1965**, *240*, 877–882.
- (45) Datiles, M.; Fukui, H.; Kuwabara, T.; Kinoshita, J. H. Galactose Cataract Prevention with Sorbinil, an Aldose Reductase Inhibitor: A Light Microscopic Study. *Invest. Ophthalm. Vis. Sci.* **1982**, *22*, 174–179.
- (46) Simard-Duquesne, N.; Greselin, E.; Gonzales, R.; Dvornik, D. Prevention of Cataract Development in Severely Galactosemic Rats by the Aldose Reductase Inhibitor, Tolrestat (42048). *Proc. Soc. Exp. Biol. Med.* **1985**, *178*, 599–605.
- (47) Shizuo, A.; Chie, K.; Takaharu, O.; Yoshitada, N. Effect of Instillation of Aldose Reductase Inhibitor FR74366 on Diabetic Cataract. *Invest. Ophthalm. Vis. Sci.* **1991**, *32*, 3078–3083.
- (48) Frisch, M. J.; Trucks, G. W.; Schlegel, H. B.; Scuseria, G. E.; Robb, M. A.; Cheeseman, J. R.; Montgomery, J. A., Jr.; Vreven, T.; Kudin, K. N.; Burant, J. C.; Millam, J. M.; Iyengar, S. S.; Tomasi, J.; Barone, V.; Mennucci, B.; Cossi, M.; Scalmani, G.; Rega, N.; Petersson, G. A.; Nakatsuji, H.; Hada, M.; Ehara, M.; Toyota, K.; Fukuda, R.; Hasegawa, J.; Ishida, M.; Nakajima, T.; Honda, Y.; Kitao, O.; Nakai, H.; Klene, M.; Li, X.; Knox, J. E.; Hratchian, H. P.; Cross, J. B.; Bakken, V.; Adamo, C.; Jaramillo, J.; Gomperts, R.; Stratmann, R. E.; Yazyev, O.; Austin, A. J.; Cammi, R.; Pomelli, C.; Ochterski, J. W.; Ayala, P. Y.; Morokuma, K.; Voth, G. A.; Salvador, P.; Dannenberg, J. J.; Zakrzewski, V. G.; Dapprich, S.; Daniels, A. D.; Strain, M. C.; Farkas, O.; Malick, D. K.; Rabuck, A. D.; Raghavachari, K.; Foresman, J. B.; Ortiz, J. V.; Cui, Q.; Baboul, A. G.; Clifford, S.; Cioslowski, J.; Stefanov, B. B.; Liu, G.; Liashenko, A.; Piskorz, P.; Komaromi, I.; Martin, R. L.; Fox, D. J.; Keith, T.; Al-Laham, M. A.; Peng, C. Y.; Nanayakkara, A.; Challacombe, M.; Gill, P. M. W.; Johnson, B.; Chen, W.; Wong, M. W.; Gonzalez, C.; Pople, J. A. *Gaussian 03*, revision C.02; Gaussian, Inc.: Wallingford, CT, 2004.
- (49) Morris, G. M.; Goodsell, D. S.; Halliday, R. S.; Huey, R.; Hart, W. E.; Belew, R. K.; Olson, A. J. Automated Docking Using a Lamarckian Genetic Algorithm and Empirical Binding Free Energy Function. *J. Comput. Chem.* **1998**, *19*, 1639–1662.
- (50) Huey, R.; Morris, G. M.; Olson, A. J.; Goodsell, D. S. A Semiempirical Free Energy Force Field with Charge-Based Desolvation. *J. Comput. Chem.* **2007**, *28*, 1145–1152.
- (51) SYBYL 7.3, *Molecular Modeling System*; Tripos Inc.: St. Louis, MO, 2006.
- (52) Head, J.; Zerner, M. C. A Broyden-Fletcher-Goldfarb-Shannon Optimization Procedure for Molecular Geometries. *Chem. Phys. Lett.* **1985**, *122*, 264–274.

JM701613H